

Why Microtubules run in Circles - Mechanical Hysteresis of the Tubulin Lattice

Falko Ziebert,^{1,2} Hervé Mohrbach,^{3,2} and Igor M. Kulić²

¹Albert-Ludwigs-Universität, 79104 Freiburg, Germany

²Institut Charles Sadron UPR22-CNRS, 67034 Strasbourg, France

³Groupe BioPhysStat, LCP-A2MC, Université de Lorraine, 57078 Metz, France

The fate of every eukaryotic cell subtly relies on the exceptional mechanical properties of microtubules. Despite significant efforts, understanding their unusual mechanics remains elusive. One persistent, unresolved mystery is the formation of long-lived arcs and rings, e.g. in kinesin-driven gliding assays. To elucidate their physical origin we develop a model of the inner workings of the microtubule's lattice, based on recent experimental evidence for a conformational switch of the tubulin dimer. We show that the microtubule lattice itself coexists in discrete polymorphic states. Curved states can be induced via a mechanical hysteresis involving torques and forces typical of few molecular motors acting in unison. This lattice switch renders microtubules not only virtually unbreakable under typical cellular forces, but moreover provides them with a tunable response integrating mechanical and chemical stimuli.

PACS numbers: 87.16.Ka, 82.35.Pq, 87.15.-v

Microtubules (MTs) are the stiffest cytoskeletal component and play many versatile and indispensable roles in living cells. As 'cellular bones', they define to a large part cell mechanics, and are crucial for cellular transport and cell division [1–4]. Beyond their biological importance, MTs have been used as molecular sensors for intracellular forces, as biotemplates for nanopatterning, and as building blocks for hybrid materials and active systems like artificial cilia and self-propelled droplets [5–10]. The MT's structure is well known [11]: the elementary building blocks, tubulin dimers, polymerize head to tail into linear protofilaments, that associate side by side to form the hollow tube structure known as the MT.

Despite of the MTs' importance, widespread use, the knowledge of its structure, and numerous experiments probing their elastic properties [13–17], understanding their basic mechanics still poses challenging problems. A remarkable one is found in MT gliding assays [18–21], see Fig. 1: already two decades ago, Amos & Amos [19] observed that MTs driven by kinesin motors on a glass surface can form arcs which continue gliding for significant time intervals before suddenly straightening out. They remarked with quite some foresight that these circular MT states could be explained by the existence of alternative tubulin dimer conformations [22]. The observation remained without wider public notice despite the frequent reoccurrence of MT arcs in the gliding dynamics of single filaments [23–25], bundles [26–28] and in collective (high density) gliding [29]. Force-induced circular arcs on the same scale, but rather dissimilar to classical buckling, have been found in numerous other situations [20, 30], also *in vivo* [31–33]. While the lifetime of MT rings varies, their characteristic size of about one micron is preserved in single filament experiments [19, 23–25], indicating a robust mechanism at work. The importance of internal degrees of freedom of the MT lattice (e.g. interprotofilament shear [34, 35] and tubulin conformational

switching [36]) has been recently stressed in explaining another MT 'anomaly', the surprising length dependent stiffness in clamped MT experiments [16, 17]. However, the formation of long lived, highly curved states or rings could not be rationalized so far. We here present a model of MT mechanics that integrates the current experimental knowledge. It shows that under external forces, MTs can be converted into metastable circular states, explaining the recurrent observations of gliding rings.

Switchable Tube Model. We will develop a simple yet generic elastic model of MTs that principally revises their mechanical response. We make use of the following experimental facts about tubulin and the MT lattice [37]. Fact 1: The protofilament can coexist in at least two conformational states [38], one of them straight, the other one highly curved with radius of curvature 20-30 nm [38–40]. Fact 2: The MT lattice displays two elongational states with one of them being about 2% shorter [41]. The MT is modeled, cf. Fig. 2a, as a bi-layered tubular structure with an inner and an outer layer of material both together representing the coarse-grained lattice of tubulin dimers. We parameterize the MT cross-section by the azimuthal angle ϕ and the radial distance R to the centerline. For a MT containing N protofilaments

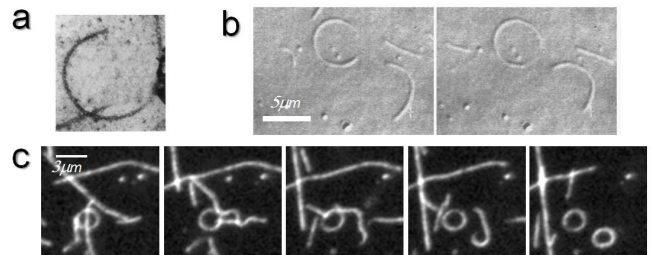


FIG. 1. (a)-(c) Mysterious ring formation of microtubules gliding on a kinesin motor carpet. From [19],[23] and [25], respectively.

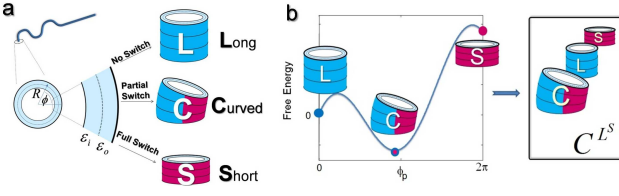


FIG. 2. (a) The bistable tube model with internal prestrains leading to three different lattice states: short and straight ("S"), long and straight ("L") and curved ("C"). (b) A typical polymorphic energy landscape, cf. Eq. (2), with three metastable states and the associated polymorphic signature (with C the ground state, L and S "excited" states).

(typically 13), a circumferential block of p consecutive dimers is hence given by $\phi \in [0, \frac{2\pi p}{N}]$, $R \in [R_i, R_o]$, with $R_{i,o}$ the inner and outer MT radii known from crystallography [1]. If the tube were to be intrinsically relaxed and preferentially straight, once it is bent or stretched it will endure inner strains, in the simplest case via a combination of pure stretching and geometric curvature contributions, $\varepsilon(R, \phi) = -\vec{\kappa} \cdot \mathbf{R} + \bar{\varepsilon}$. Here $\vec{\kappa}$ is the vectorial curvature and $\bar{\varepsilon}$ the mean stretching strain of the cross-section. The conformational 'polymorphic' state of a tubulin is described by a variable σ , assuming one of two states: straight, with $\sigma = 0$ and vanishing preferred strain $\varepsilon_{pref} = 0$, and curved with $\sigma = 1$ generating finite prestrain. In general the prestrain has different values $\varepsilon_{pref} = \varepsilon_i$ or ε_o in the two layers, see Fig. 2a.

The energy density of the MT's cross-section consists of two parts: the elastic energy (with Y Young's modulus) $e_{el} = \frac{Y}{2} \int_{R_i}^{R_o} dr \int_0^{2\pi} r d\phi [\varepsilon(r, \phi) - \varepsilon_{pref}(r, \phi)]^2$. Second, each dimer can reduce its free energy by $|\Delta G|$ by switching to the curved state. The respective energy of the cross-section is $e_{switch} = \frac{\Delta G}{b} \sum_{n=1}^N \sigma_n$ with $b \approx 8$ nm the tubulin size. A negative free energy, $\Delta G < 0$, will favor the curved state. Within the lattice, however, dimer switching competes with the elastic energy. A tube section with a block of dimers switched to the curved state will endure prestress that can be (partially) relieved by global tube deformations: the MT will show axial shortening/lengthening and, remarkably for the observer, curving. External forces, F , and torques, M , give rise to additional couplings. The total energy $e_{tot} = e_{el} + e_{switch}$ can be calculated to be [42]

$$\tilde{e}_{tot} = \frac{\kappa^2}{2} + \frac{a_0 \bar{\varepsilon}^2}{2} - \kappa \sin \frac{\phi_p}{2} + a_1 \phi_p \bar{\varepsilon} + m \kappa + \lambda \bar{\varepsilon} + \gamma \phi_p, \quad (1)$$

where we scaled curvature by its characteristic value κ_1 , energy by $B\kappa_1^2$, torque like $m = M/B\kappa_1$ and tension like $\lambda = F/B\kappa_1^2$. The newly introduced variable $\phi_p = 2\pi p/N$ is the angular size of the switched block, to which we refer to as the 'polymorphic variable' in the following. It is this inner variable of the lattice, that is often concealed from observation but can give rise to surprising effects. The characteristic curvature κ_1 is completely determined

by the known tube dimensions and the prestrains. Using the experimental facts 1 & 2, we estimate the preferred strains to be $\varepsilon_i = 0.7 \cdot 10^{-2}$ and $\varepsilon_o = -3.3 \cdot 10^{-2}$, see [42] for details. κ_1 will set the scale for the gliding arcs and rings. As an important cross-check, using the estimated strain values we get $\kappa_1 \simeq 1.1 \mu\text{m}^{-1}$, consistent with the experimental observations [19, 23–25]. The first two terms in Eq. 1 are of purely elastic origin, the next two are cross-coupling terms between elastic and polymorphic variables, and the last three are related to the action of generalized forces. $\gamma = a_2 + \frac{N\Delta G}{2\pi b B\kappa_1^2}$ is the effective energy density of switching; it consists of an elastic penalty due to the lattice constraint, a_2 , and of the free energy difference per length, $\Delta G/b$, due to switching. a_0, a_1 and a_2 are completely determined dimensionless constants [42].

To carve out the features of this energy, we first consider imposed external force and torque. A minimization with respect to strain $\bar{\varepsilon}$ and curvature κ yields

$$e_{tot}(\phi_p) = -\frac{c_p}{2} \phi_p^2 + f \phi_p - m \sin \frac{\phi_p}{2} - \frac{1}{2} \sin^2 \frac{\phi_p}{2}, \quad (2)$$

a function of torque m and effective tension $f = \gamma - c_f \lambda$. For the given prestrains $\varepsilon_{i,o}$ we estimate the dimensionless constants $c_p \simeq 0.1$, $c_f \simeq 2.5 \cdot 10^{-3}$, and γ between 0 and 1 for $|\Delta G|$ of the order of several kT, see [42] for details. The generalized force is a function of lattice geometry and tension, and most importantly of the switching energy, i.e. $f = f(\Delta G)$.

Eq. (2) is the central result: it describes the energy of a MT cross-section with partially switched tubulins and contains all the information needed to characterize the mechanical behavior of MTs under external loads. As a function of the acting force and torque, the 'state diagram' of a MT cross-section displays a number of distinct regions: the energy landscape can exhibit one, two or three local minima, cf. Fig. 2b. The states corresponding to these minima are a long straight state (denoted with "L") with $\phi_p = 0$, a short straight state ("S") with $\phi_p = 2\pi$ and a curved state ("C") having an intermediate value $0 < \phi_p < 2\pi$. For further discussion we introduce an intuitive notation (*polymorphic signature*) capturing both the energy shape and the actual state, taking one of these forms: a single mechanically stable state X , two X^Y or three stable states $X^Y Z$ (with X, Y, Z either one of S, L, C). Increasing energy values are indicated by ascending indices and the actual state by underlining the corresponding index. For instance, in $\underline{X}^Y Z$ the ground state X is populated, while in $X^{\underline{Y}} Z$ metastable state Y .

The complete variety of polymorphic signatures physically allowed by e_{tot} for given torque m and effective force f is summarized in the 'polymorphic state diagram' in Fig. 3. Note that the simple model – considering two dimer states – leads to an extremely rich lattice behavior. There is an intrinsic symmetry with respect to the vertical line given by $f = \pi c_p$ and passing through the point

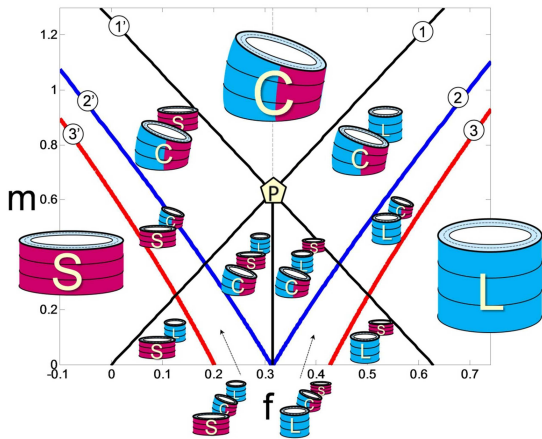


FIG. 3. The polymorphic state diagram for a MT cross-section as a function of effective force f and torque m , cf. Eq. (2). The diagram depends on the parameter c_p , estimated from the experimental measurements of protofilament curvature and MT lattice shortening (cf. main text).

P: a mirror operation with respect to this line transforms the two straight states S and L into each other, leaving the curved state invariant. We will hence restrict the discussion to MTs initially in the L state. The most interesting, ‘polymorphically curved region’, i.e. the range where stable or metastable curved states occur, is comprised between the two red curves, ③ and ③’. Outside of these curves, the behavior is *indistinguishable* from the one of a simple elastic beam or worm-like chain (WLC). Between the two blue curves, ② and ②’, the curved state C has lowest energy. Moreover, in the region above the point P and between the two black lines ① (given by $m = 2f$) and ①’, the curved state C is even the *only* existing state. Finally, MTs are most sensitive to external loads close to point P , where the curved state is the ground state in all surrounding regions. One expects ‘polymorphic behavior’ – i.e. (parts of) MTs curved as in Fig. 1 – to become visible when the respective cross-sections are mechanically converted to the C state. From the state diagram the necessary torque for this conversion, depending also on the force, can be estimated to be of the order of $10 \text{ pN}\mu\text{m}$ (corresponding to $m = 1$ in reduced units). As a single kinesin motor exerts forces of 2-5 pN [1] on MTs with typical radius of curvature of $1\mu\text{m}$, this provides us with a first clue for understanding the MT’s propensity to form rings in gliding assays, even when motor coverage on the substrate is moderate.

Gliding-induced Ring Formation. To investigate whether the found polymorphic signatures, emerging from the switchable internal structure of the MT, indeed explain ring formation, we generalized previous gliding assay modeling [21, 43] and simulated buckling events of gliding MTs. Due to the confinement by the motors,

the MT can be described by a 2D space curve $\mathbf{r}(s)$. We assume that the MT’s shape and the inner polymorphic variable $\phi_p(s)$ both follow relaxational dynamics

$$\dot{\mathbf{r}} = \begin{pmatrix} \mathbf{nn} & \mathbf{tt} \\ \xi_{\perp} & \xi_{\parallel} \end{pmatrix} \cdot \left[-\frac{\delta E}{\delta \mathbf{r}} + f_m \mathbf{t} \right], \quad \dot{\phi}_p = -\frac{1}{\zeta} \frac{\delta E}{\delta \phi_p}, \quad (3)$$

given by the polymorphic energy

$$E = \int_0^L ds \left[B\kappa_1^2 \tilde{e}_{tot} + \frac{1}{2} (\mathbf{t}^2 - 1) \lambda + \frac{B_p}{2} (\partial_s \phi_p)^2 \right], \quad (4)$$

augmented by a length constraint (introducing the Lagrangian multiplier $\lambda(s)$) and a term penalizing variations in the polymorphic variable along the arc length. The latter introduces a polymorphic stiffness parameter, B_p , modeling a certain cooperativity in lattice switching [36, 44]. In the dynamic equations, ξ_{\perp} and ξ_{\parallel} are anisotropic friction coefficients related to motor friction, and ζ is associated to dissipation in the switching. f_m is the local force density exerted by the kinesin motors attached to the substrate, transporting the filament along the local tangent \mathbf{t} . More details can be found in [42].

What happens if an initially straight MT gets stuck and buckles due to the action of motors? The answer depends on torque and force, varying in the course of buckling as follows (cf. blue curve in Fig. 4d): initially, the MT is gliding freely, $f = \gamma$. Upon getting stuck, compressive tension is rapidly created leading quasi-instantaneously to $f = \gamma - c_f \lambda$, followed by a slower build-up of torque due to the emerging curvature. As long as the MT tip remains stuck the torque increases while tension partially relaxes via buckling, see the part of the blue curve in Fig. 4d with the arrow pointing upwards. Once the MT tip is released, the torque relaxes and one finally ends up at the starting point at $f = \gamma$ and $m \simeq 0$. This ‘loop’ in the state diagram broadens and extends to higher torque values with increasing motor force f_m . Depending on the effective tension and torque induced during buckling, several distinct scenarios are possible:

For negligible dimer switching energies $\Delta G \simeq 0 \text{ kT}$ ($\gamma \simeq 1$) or positive ones, a MT initially in the L state buckles as a classical semiflexible filament (WLC) as shown in Fig. 4a: buckles with force-dependent curvature emerge close to the tip and straighten again after unsticking. The same behavior is found for strongly negative values of $\Delta G \lesssim -15 \text{ kT}$ ($\gamma \simeq -0.4$), and a MT starting out from state S . In both cases, the induced torques are insufficient for crossing curve ① or ①’, consequently the MT remains in the stable L (or S) state.

For intermediate values of dimer switching energies $-6.3 \text{ kT} \lesssim \Delta G \lesssim -5.1 \text{ kT}$ ($0.3 \lesssim \gamma \lesssim 0.4$) the critical line ① is crossed for high enough torques. Consequently the C state becomes populated at the filament tip, resulting in arc-like buckles with curvature $\kappa \simeq \kappa_1$, see Fig. 4b. Upon unsticking and concomitant torque decrease, state L acquires lowest energy. Remarkably, despite of L being

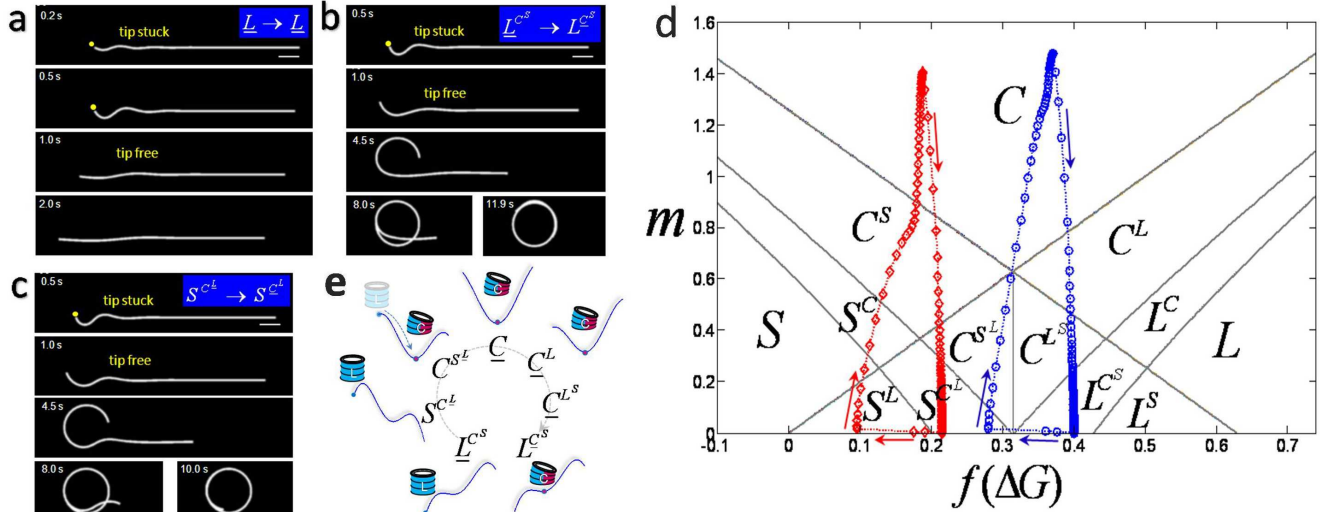


FIG. 4. Dynamic shape evolutions of gliding MTs that become temporarily stuck and buckle. All parameters are identical in a)-c), except for ΔG resulting in different effective forces f , cf. Fig. 3 and panel d. a) A MT far from the polymorphic region ($\Delta G = +1.7$ kT corresponding to $\gamma = 1$) behaves like a gliding WLC upon buckling and release. b) A MT for which the buckling induces a switch to the curved state ($\Delta G = -5.2$ kT, $\gamma = 0.4$). The finally formed ring is metastable, i.e. L has lower energy than C . c) A MT displaying multiple buckles that persist after unsticking and roll-up ($\Delta G = -7.3$ kT, $\gamma = 0.215$). d) Trajectories in the polymorphic state diagram corresponding to the dynamics shown in b (blue curve) and c (red curve), resulting in a hysteretic loop upon torque creation and release, cf. the sketch in e). Scale bars in a)-c) are $1\mu\text{m}$, gliding velocity $v = 1\mu\text{m/s}$. All parameter values can be found in [42].

the ground state, the leading buckle locks in the C state, i.e. in the metastable configuration L^{C^S} . This scenario of a closed loop in the polymorphic state diagram triggered by external forces and ending up in a metastable curved state, could be called ‘mechanical hysteresis’. The related path is shown as the blue curve in Fig. 4d and the concomitant changes in the energy landscape and the polymorphic signatures passed in Fig. 4e. Although state C is only metastable, the whole MT eventually rolls up and converts to C by simply following the motion of the tip in the course of the gliding dynamics, as shown in Fig. 4b. For dimer switching energies $-7.5\text{ kT} \lesssim \Delta G \lesssim -6.3\text{ kT}$ ($0.2 \lesssim \gamma \lesssim 0.3$) the behavior is similar as just discussed, when the initial state L is replaced by S . The MT converts into the C state upon buckling. The polymorphic signature will evolve from S^{C^L} into S^{C^L} .

Finally, Fig. 4c shows yet another scenario, that takes place when S is the ground state, yet the MT starts from the L state (red curve in Fig. 4d). Due to the polymorphic landscape, state C is populated almost immediately during buckling, buckles remain stable after unsticking and the final state is again a ring, but in state S^{C^L} .

The most sensitive parameter controlling polymorphic behavior is the free energy difference ΔG : changes in the range from 0 to -10kT fundamentally alter the response to external forces. This suggests deep impact of various binding agents, like the GTP-analogue GMPCPP

[20], MKAC [38] or tau [49], either triggering or inhibiting polymorphic behavior. Our model yields estimated bounds for ΔG : if a MT forms metastable rings our analysis implies that $-7.5\text{ kT} \lesssim \Delta G \lesssim -5\text{ kT}$.

Conclusions. We have developed a generic model that principally revises the mechanics of microtubules and explains their metastable curved states. The conceptually simple model comprises the classical semiflexible filament behavior at low loads. However, when the applied forces and torques exceed a threshold (tens of pN), MTs convert to metastable curved conformations via a mechanical hysteresis loop. The mechanically induced polymorphic switching shares similarities with bacterial flagella [45–47]. The metastability – MTs “remember” force-induced curved shapes – puts them close to man-made shape memory materials [48]. It is intriguing that already two states of the subunit give rise to a plethora of polymorphic signatures that can be triggered externally. The strong sensitivity to the transition energy shows that the design is highly versatile and could inspire novel smart materials. The major challenge will now be to unravel how the microtubule polymorphic switch is utilized in Nature.

Acknowledgements. We thank A. Johner, K.J. Böhm and D. Chrétien for stimulating discussions and A. Maloney, L. Herskowitz, and S. Koch for publishing and sharing their gliding assay image series open data. F. Z. thanks the DFG for partial support via IRTG 1642

-
- [1] J. Howard, *Mechanics of Motor Proteins and the Cytoskeleton* (Sinauer, Sunderland, 2001).
- [2] L. A. Amos and W. G. Amos, *Molecules of the Cytoskeleton* (Guilford, New York, 1991).
- [3] I. M. Kulic, et al., Proc. Natl. Acad. Sci. USA **105**, 10011 (2008).
- [4] E. Karsenti and I. Vernos, Science **294**, 543 (2001).
- [5] C. P. Brangwynne, G. H. Koenderink, F. C. MacKintosh, and D. A. Weitz, Phys. Rev. Lett. **100**, 118104 (2008).
- [6] E. Meyrhöfer and J. Howard, Proc. Natl. Acad. Sci. USA **92**, 574 (1995).
- [7] C. Reuther, L. Hajdo, R. Tucker, A. A. Kasprzak and S. Diez, Nano Lett. **6**, 2177 (2006).
- [8] L. Ionov, V. Bocharova, and S. Diez, Soft Matt. **5**, 67 (2008).
- [9] T. Sanchez, D. Welch, D. Nicastro, and Z. Dogic, Science **333**, 456 (2011).
- [10] T. Sanchez, D. T. Chen, S. J. DeCamp, M. Heymann, and Z. Dogic, Nature **491**, 431 (2012).
- [11] K. H. Downing and E. Nogales, Curr. Opin. Cell Biol. **10**, 16 (1998).
- [12] H. W. Wang and E. Nogales, Nature **435**, 911 (2005).
- [13] F. Gittes, B. Mickey, J. Nettleton, and J. Howard, J. Cell Biol. **120**, 923 (1993).
- [14] P. Venier, A. C. Maggs, M. F. Carlier, and D. Pantaloni, J. Biol. Chem. **269**, 13353 (1994).
- [15] H. Felgner, R. Frank, and M. Schliwa, J. Cell Sci. **109**, 509 (1996).
- [16] F. Pampaloni, et al., Proc. Natl. Acad. Sci. USA **103** 10248(2006).
- [17] K. M. Taute, F. Pampaloni, E. Frey, and E. L. Florin, Phys. Rev. Lett. **100** 028102 (2008).
- [18] R. D. Vale, B. J. Schnapp, T. S. Reese, and M. P. Sheetz, Cell **40** 559 (1985).
- [19] L. A. Amos and W. B. Amos, J. Cell Sci. Suppl. **14** 95 (1991).
- [20] R. D. Vale, C. M. Coppin, F. Malik, F. J. Kull, and R. A. Milligan, J. Biol. Chem. **269** 23769 (1994).
- [21] L. Bourdieu, et al., Phys. Rev. Lett. **75** 176 (1995).
- [22] C. H. Aylett, J. Löwe, and L. A. Amos, Int. Rev. Cell Mol. Biol. **292** 1 (2011).
- [23] K. J. Böhm, R. Stracke, W. Vater, and E. Unger, in *Micro- and Nanostructures of Biological Systems*, Eds. H. J. Hein and G. Bischoff (Shaker Verlag, Aachen, 2001), pp. 153-165.
- [24] P. Bieling, I. A. Telley, J. Piehler, and T. Surrey, EMBO Rep. **9** 1121 (2008).
- [25] L. Liu, E. Tüzel, and J. L. Ross, J. Phys. Condens. Matter **23** 374104 (2011).
- [26] R. Kawamura, A. Kakugo, K. Shikinaka, Y. Osada, and J. P. Gong, Biomacromolecules **9** 2277(2008).
- [27] H. Hess, et al., Nano Lett. **5** 629 (2005).
- [28] I. Luria, et al., Soft Matt. **7** 3108 (2011).
- [29] Y. Sumino, et al., Nature **483** 448 (2012).
- [30] A. Maloney, L. J. Herskowitz, and S. J. Koch, PLoS ONE **6** e19522 (2011).
- [31] T. J. Keating, J. G. Peloquin, V. I. Rodionov, D. Momcilovic, G. G. Borisy, Proc. Natl. Acad. Sci. USA **94** 5078 (1997).
- [32] A. D. Bicek, E. Tüzel, D. M. Kroll, D. J. Odde, in *Methods in Cell Biology*, Eds. Y. Wang and D. E. Discher (Elsevier, Amsterdam, 2007), pp. 237-268.
- [33] C. P. Brangwynne, et al., J. Cell Biol. **173**733 (2006).
- [34] C. Heussinger, M. Bathe, and E. Frey, Phys. Rev. Lett. **99** 048101 (2007).
- [35] H. Mohrbach and I. M. Kulic, Phys. Rev. Lett. **99** 218102 (2007).
- [36] H. Mohrbach, A. Johnner, and I. M. Kulic, Phys. Rev. Lett. **105** 268102 (2010).
- [37] These facts were established for taxol stabilized protofilaments/MTs, a protocol also used in the majority of the gliding experiments.
- [38] C. Elie-Caille, et al., Curr. Biol. **17** 1765(2007).
- [39] T. Müller-Reichert, D. Chrétien, F. Severin, and A. A. Hyman, Proc. Natl. Acad. Sci. USA **95**:3661 (1998).
- [40] Note that in [38] a third, less curved state with radius of curvature of 250 nm was also detected, which we neglect here as the MT shape will be dominated by the highly curved state.
- [41] I. Arnal and R. H. Wade, Curr. Biol. **5** 900 (1995).
- [42] More details can be found in the supplementary informations, EPAPS= (will be added by editor).
- [43] F. Nedelec, D. Foethke, New J. Phys. **9** 427 (2007).
- [44] H. Mohrbach, A. Johnner, and I. M. Kulic, Eur. Biophys. J. **41** 217 (2012).
- [45] N. C. Darnton and H. C. Berg, Biophys. J. **92** 2230 (2007).
- [46] S. V. Srigiriraju and T. R. Powers, Phys. Rev. Lett. **94**, 248101 (2005).
- [47] H. Wada and R. R. Netz, EPL **82**, 28001 (2008).
- [48] K. Bhattacharya, *Microstructure of Martensite: Why It Forms and How It Gives Rise to the Shape-Memory Effect* (Oxford University Press, Oxford, 2003).
- [49] A. Samsonov, J. Z. Yu, M. Rasenick, and S. V. Popov, J. Cell Sci. **117** 6129 (2004).